Bulk ordering and surface segregation in $Ni_{50}Pt_{50}$

L. V. Pourovskii,[1,2] A. V. Ruban,[3] I. A. Abrikosov,[1] Y. Kh. Vekilov,[2] and B. Johansson[4]

[1]*Condensed Matter Theory Group, Physics Department, Uppsala University, Box-530, S-75121 Uppsala, Sweden*

[2]*Theoretical Physics Department, Moscow Steel and Alloys Institute, 117419, 4 Leninskii pr., Moscow, Russia*

[3]*Center for Atomic-scale Materials Physics and Physics Department, Technical University of Denmark, DK-2800 Lyngby, Denmark*

[4]*Applied Materials Physics, Department of Materials, Science and Engineering, Royal Institute of Technology,*

SE-100 44 Stockholm, Sweden

Interatomic interactions obtained from the effective screened generalized-perturbation method have been applied in Monte Carlo simulations to derive the bulk and surface-alloy configurations for $Ni_{50}Pt_{50}$. The calculated order-disorder transition temperature and short-range order parameters in the bulk compare well with experimental data. The surface-alloy compositions for the (111) and (110) facets above the ordering transition temperature are also found to be in a good agreement with experiments. It is demonstrated that the segregation profile at the (110) surface of NiPt is mainly caused by the unusually strong segregation of Pt into the second layer and the interlayer ordering due to large chemical nearest-neighbor interactions.

I. INTRODUCTION

The surface composition of the NiPt alloy system has been the subject of intensive theoretical as well as experimental investigations for the last two decades. One of the reasons for the interest is the unique orientation dependence of the surface segregation: As first revealed by Gauthier *et al.*,[1,2] the topmost layers of the (111) and (100) surfaces of the NiPt alloy are enriched by Pt, while there is a strong Ni segregation toward the (110) surface. Subsequent experimental investigations by low-energy electron diffraction (LEED), ion-scattering spectroscopy, incidence-dependent excitation for Auger spectroscopy (IDEAS) (Refs. 3–10) of alloys with different composition ($Pt_{10}Ni_{90}$, $Pt_{25}Ni_{75}$, $Pt_{50}Ni_{50}$) have confirmed the initial conclusion: In the NiPt alloy Pt segregates toward the (100) and (111) topmost surface layers, while there is a reversed segregation at the (110) surface, which is almost entirely covered by Ni.

Up to date the theoretical investigations of an orientation-dependent surface segregation in NiPt have been mostly confined to semiempirical approaches. Earlier embedded-atom method (EAM) (Refs. 4 and 11) and tight-binding Ising model (Refs. 12 and 13) calculations predicted Pt segregation toward the (110) surface for a measured concentration range of 10–50 at. % Pt, thus failing completely to reproduce the segregation reversal phenomenon. Recent EAM calculations with parameters derived specifically for the NiPt alloys[14] and empirical calculations by Hofer and Mezey[15] give results in agreement with experiment.

Results from first principles were obtained by Abrikosov *et al.*[16] who used the surface version of the Connolly-Williams (CW) method[17,18] to extract effective interatomic interactions from the total energies of different random-surface alloys. This was obtained by the linear muffin-tin orbital (LMTO) Green's-function (GF) method in the atomic-sphere (ASA) and coherent-potential approximations (CPA) (Refs. 19 and 20), and, then derived interactions were used in single-site, mean-field statistical thermodynamics simulations. The concentration profiles for the (111), (110), and (100) surfaces obtained in this way agreed fairly well

with the experimental data, and the authors concluded that the segregation reversal at the (110) surface was caused by a strong segregation of Pt towards the second layer in combination with a tendency to form a structure of alternating Pt and Ni layers at this surface.

Although no adjustable parameters were used in those calculations, they involved several assumptions and approximations that limited the accuracy of the results. First of all, as it is clear now,[21,22] the screening contribution to the Madelung potential and energy in the single-site approximation was overestimated. This led to a lowering of the total energy of the random alloys and as a result to an overestimate of the effective pair interactions, which were obviously too high, for instance, to reproduce correctly the order-disorder transition in NiPt.

Another approximation employed in this earlier work was the use of effective interactions restricted to the first coordination shell in the expansion of the total energy, as dictated by the use of only random alloys in the CW method. If more distant interactions are not negligible, they indirectly renormalize the nearest-neighbor interactions introducing an additional error. In a single-site mean-field calculation of the surface-concentration profiles, which neglect all short-range order and correlation effects, like the treatment in Ref. 16, this does not matter since the CW interactions in this case are just coefficients of the total energy expansion in terms of the alloy concentration in different layers. However, such interactions cannot be used in the more accurate Monte Carlo (MC) simulations. The latter are needed in the presence of pronounced ordering effects that the single-site mean-field approximation highly overestimates for fcc alloys.[37]

Therefore, to verify the results of Ref. 16 we apply here a completely different computational technique, both for obtaining the effective cluster interactions and for the statistical thermodynamic simulations. In particular, the effective cluster interactions are obtained by the screened generalized-perturbation method (SGPM) that takes into account the screened Coulomb interaction contribution to the configurational energy in the cases where the net charges of the alloy components are not electroneutral. Although in this case one

is again restricted by the use of the single-site and coherent-potential approximations, this scheme seems to be the only practical way of calculating effective interactions in inhomogeneous systems where distant interactions are not negligibly small. This is so since the use of the CW method for open surfaces like fcc(110) involves a great number of calculations (equal at least to the number of different interactions) of the huge supercells which should be big enough not only in the direction pependicular to the surface, but also parallel to the surface in order to provide *intralayer* decomposition of the total energy in terms of interatomic interactions.

To calculate the surface-concentration profiles we use a direct-exchange Monte Carlo (DEMC) method, which allows us to calculate the equilibrium surface concentration profile for a fixed bulk composition in the Grand canonical ensemble. The lattice relaxation effects, which play an important role in the thermodynamics of NiPt alloys are treated in the effective tetrahedron volume approach similar to the one proposed by Amador *et al.*[23] Before we proceed to the calculation of the surface-concentration profiles we first check whether these schemes and the SGPM interactions can correctly reproduce the ordering in the bulk. We also compare the SGPM interactions in bulk NiPt with the corresponding CW interactions obtained from total energy calculations by the Korringa-Kohn-Rostoker–ASA with multipoles (KKR-ASA+M).

The present paper is organized as follows: in Sec. II we describe the applied methods and details of the calculations. In Sec. III we present our results for the thermodynamic properties of ordered and random $Ni_{50}Pt_{50}$ alloys as well as the results of the Monte Carlo simulations for the order-disorder transition temperature and short-range order (SRO) parameters in the disordered state. The calculated segregation energies and surface effective interatomic potentials are presented in Secs. IV and V, respectively. The calculated segregation profiles for the (110) and (111) surfaces of the $Ni_{50}Pt_{50}$ alloy are presented and discussed in Sec. VI.

II. COMPUTATIONAL TECHNIQUES

In this work we have employed a number of different computational techniques. The total energy calculations for bulk and surface NiPt alloys were carried out in the framework of the density-functional theory[24] (DFT) using the KKR-ASA Green's-function method.[25] Electronic structure calculations for disordered alloys were done within the coherent-potential approximation.[26–28] The multipole moment correction to the ASA Madelung one-electron potential and total energy (ASA+M) Refs. 19 and 29 have been used in all our calculations. The effective interactions have been obtained by the screened generalized-perturbation method[22] and the Connolly-Williams method[17] in the bulk. The statistical thermodynamic simulations have been carried out by the Monte Carlo method for the bulk alloy and the direct-exchange Monte Carlo method for the surfaces.

A. Density functional theory calculations

The KKR-CPA-ASA+M Green's-function method have been applied to the bulk and surface DFT calculations of the

NiPt alloys. This method is described in details in Refs. 20, 30, and 31. Surface calculations have been carried out using both a semi-infinite geometry with the surface Green's-function technique and a supercell approach. The basis functions have been truncated at $l_{max}=3$, which allowed us to use the multipole moments up to $2l_{max}+1$ in the multipole Madelung potential and energy. As has been shown in Ref. 30 this leads in particular to a more accurate description of the inhomogeneous systems and allows one, for instance, to reproduce properly the surface energies of metals and their anisotropy which is important in the case of the (110) surface. The local Airy gas (LAG) approximation[32] has been used for the exchange-correlation energy.

Since $Ni_{50}Pt_{50}$ is paramagnetic,[33] all the calculations were spin-restricted. We have used the scalar-relativistic approximation[34] throughout our study. The screening contribution to the Madelung potential and energy in the single-site approximation has been taken into account as described in Ref. 22. We have also included the so-called muffin-tin correction to the electrostatic energy,[35] which substantially improves the results for the equilibrium lattice spacing.

The energy integration was carried out in the complex plane on a semicircular contour comprising 16 energy points. We have used 505 k points in the irreducible part of the fcc Brillouin zone for the bulk calculations and 64 and 90 k points in the irreducible part of the two-dimensional Brillouin zones for the (110) and (111) surfaces, respectively, in the surface Green's-function calculations. The thickness of the principal layer is equal to 5 layers for the (110) surface and 3 layers for the (111) surface.

B. Cluster expansion of the total energy

The statistical thermodynamics simulations require the knowledge of the total energy of the alloy on a fixed lattice as a function of the atomic configuration. In the case of a binary alloy the atomic configuration can be represented by spin variables σ_i taking on values $+1$ or -1 depending on the type of atom occupying site i. The average products of the spin variables, $\langle \sigma_i \sigma_j \ldots \sigma_k \rangle$, are the multisite correlation functions that form the complete basis for the total energy expansion[36] in terms of the effective cluster interactions,

$$E_{tot}=V^{(0)}+V^{(1)}\langle\sigma\rangle+\sum_s V^{(2,s)}\langle\sigma_i\sigma_j\rangle^s$$

$$+\sum_s V^{(3,s)}\langle\sigma_i\sigma_j\sigma_k\rangle^s+\cdots, \qquad (1)$$

where i, j, and k are lattice sites, $V^{(0)}$ is the reference energy, which, in fact, is the total energy of a random equiatomic alloy, and $V^{(d,s)}$ is the effective cluster interaction, which corresponds to the cluster of the order d and type s. For instance, $V^{(2,1)}$, $V^{(2,2)}$, and $V^{(2,3)}$ are the effective pair interactions in the first, second, and third coordination shells, respectively. The on-site interaction $V^{(1)}$, which is the effective chemical potential, can be neglected in the canonical ensemble calculations.

In the case of inhomogeneous systems the formula (1) should be written as,

BULK ORDERING AND SURFACE SEGREGATION IN Ni$_{50}$Pt$_{50}$ . . .

PHYSICAL REVIEW B **64** 035421

$$E_{tot}^{surf} = V^{(0)} + \sum_{\lambda} \left[V_{\lambda}^{(1)} \langle \sigma_{\lambda} \rangle + \sum_{\lambda',s} V_{\lambda\lambda'}^{(2,s)} \langle \sigma_{\lambda;i} \sigma_{\lambda';j} \rangle^{s} \right.$$

$$\left. + \sum_{\lambda',\lambda'',s} V_{\lambda\lambda'\lambda''}^{(3,s)} \langle \sigma_{\lambda;i} \sigma_{\lambda';j} \sigma_{\lambda'';k} \rangle^{s} + \cdots \right], \quad (2)$$

where the effective interactions $V_{\lambda\lambda'\lambda''}^{(d,s)} \ldots$ now depend not only on the cluster order d and its type s, but also on the relative position of the cluster $\lambda\lambda' \ldots$, which designates those atoms of the cluster that are located in layers λ, λ', λ'', and so on. The contribution from the on-site interactions

$$V_{\lambda}^{(1)} = \mu_{\lambda}, \quad (3)$$

which is the chemical potential in the λ layer, must also be taken into consideration in the calculation of the surface-concentration profiles.

C. The effective SGPM interactions

The effective interactions in this work have been obtained by SGPM. In contrast to GPM usually applied in first-principles calculations,[37–39] SGPM includes the contribution from the screened Coulomb interactions to the *pair* effective interactions as described in Ref. 22. Neglecting the renormalization of the one-electron energy term due to screening, such SGPM pair interactions in the bulk may be written as

$$\tilde{V}^{(2,s)}(\sigma) = \tilde{V}_{GPM}^{(2,s)}(\sigma) + \alpha^{(2,s)} \frac{\Delta Q^2}{S}, \quad (4)$$

where $\tilde{V}_{GPM}^{(2,s)}$ is the usual GPM potential and the last term defines the contribution from the screened Coulomb interactions. It depends on the coefficients $\alpha^{(2,s)}$ that can be determined in the supercell calculations, the effective charge transfer $\Delta Q = Q_A - Q_B$, which is the difference between the net charges of the atomic spheres of the A and B components,[40] and the WS sphere radius S. In the case of fcc Ni$_{50}$Pt$_{50}$ random alloy, for instance, the coefficients $\alpha^{(2,s)}$ [in Ry units and for the spin-variable representation of the total energy, Eq. (1)] for the first four coordination shells are equal to 0.192, -0.001, -0.030, and -0.007, respectively. In a similar way one can determine contributions to the layer-resolved interactions at the surface $\tilde{V}_{\lambda\lambda'}^{(d,s)} \ldots$ that approach the values of the corresponding bulk interactions $\tilde{V}^{(d,s)}$ within the first few layers.

The one-electron contribution to the SGPM interactions, $\tilde{V}_{GPM}^{(2,s)}(\sigma)$, has been calculated in the framework of the KKR-CPA-ASA+M method. In the case of surfaces we have used a supercell geometry: A 16-layer orthorhombic supercell (11 layers of the alloy and 5 layers of vacuum) to simulate the (110) surface and a 12-layer hexagonal supercell (9 layers of the alloy and 3 layers of vacuum) to simulate the (111) surface. Fifty-one k points were used in the irreducible part of the orthorhombic Brillouin zone and 32 k points were used in the irreducible part of the hexagonal Brillouin zone for (110) and (111) supercell, respectively. The complete procedure of the determination of the screening contribution to the one-electron potential is described in Ref. 22.

The SGPM as well as GPM interactions depend on the surface composition. Therefore their use in simulations that allow for variation of the surface composition, in general requires an iterative determination of the interactions during the calculation of a self-consistent concentration profile. However, one can easily obtain the concentration (and surface composition) independent interactions by using the following relationship:[41]

$$\tilde{V}^{(n,s)}(\langle \sigma \rangle) = V^{(n,s)} + \langle \sigma \rangle V^{(n+1,s')} + \frac{\langle \sigma \rangle^2}{2} V^{(n+2,s'')} + \cdots, \quad (5)$$

where s' and s'' clusters include the lower order s cluster. It follows from Eq. (5) that for $\langle \sigma \rangle = 0$ the GPM or SGPM interactions are equal to the corresponding concentration-independent interactions obtained by the Connolly-Williams method. Thus, all our SGPM calculations have been performed for equiatomic alloys.

D. The Connolly-Williams method for the bulk

In order to verify the SGPM interactions we have obtained the corresponding interactions by means of the Connolly-Williams method in which we have used the total energies of 12 fcc-based ordered structures: fcc(Ni,Pt), L1$_2$(Ni,Pt), DO$_{22}$(Ni,Pt), Z1(Ni,Pt), L1$_0$, CH, DH, and Z2. For all these structures a unit cell with 8 atoms (double fcc unit cell) of tetragonal symmetry can be used thereby avoiding numerical uncertainties in the Brillouin zone integration. The description of L1$_2$, DO$_{22}$, L1$_0$, CH, and Z2 structures can be found in Ref. 42. Z1 (A$_3$B and B$_3$A) is a (100) layer structure, similar to the L1$_0$ and Z2 structures, but with 3 layers of one type of atoms and 1 layer of the other type. DH is similar to the CH structure, but the types of atoms in the middle (100) plane are interchanged.

The total energy calculations for these structures have been performed by the KKR-ASAM methods. In this case 275 k points in the irreducible part of the tetragonal Brillouin zone and 16 energy points on a semicircular contour in the complex plane were used for the Brillouin zone and energy integration, respectively. For all structures the lattice parameter has been taken to be equal to the calculated lattice parameter of the disordered Ni$_{50}$Pt$_{50}$ alloy.

E. Chemical potentials or on-site interactions

One of the drawbacks of the SGPM and GPM methods is that they cannot be used in the calculations of partial molar quantities, since the renormalization of the effective medium due to variation of the alloy composition is absent.[43] Thus the on-site interactions, $V_{\lambda}^{(1)}$, which are needed for the surface segregation calculations must be obtained in direct total energy calculations for alloys with different compositions. In this work we have used the KKR-CPA-ASAM surface Green's-function method[19,20,30] to obtain $V_{\lambda}^{(1)} - V_{bulk}^{(1)}$. These quantities are the segregation energies of one of the alloy components in the completely and uniformly +random equiatomic alloy with $\langle \sigma_1 \rangle = \langle \sigma_2 \rangle = \cdots = \langle \sigma_{\lambda} \rangle = \cdots = \langle \sigma_{bulk} \rangle = 0$:

$$V_\lambda^{(1)} - V_{bulk}^{(1)} = \left. \frac{dE_{surf}(\langle\sigma_\lambda\rangle)}{d\langle\sigma_\lambda\rangle} \right|_{\langle\sigma_\lambda\rangle=0}. \qquad (6)$$

F. Effective tetrahedron volume approach for lattice relaxation effects

The SGPM interactions define the configurational energy of an alloy on a fixed lattice. However, it is well known[23,44] that a large size difference between the alloy species, as in the case of Ni and Pt, leads to lattice relaxations. The lattice relaxation effects can be incorporated directly in the Connolly-Williams method,[44,45] but in the case of the SGPM interactions they require a separate treatment. In this work we have employed an approach which is very similar to the effective-cluster volume scheme proposed by Amador et al.[23]

We assume that the tetrahedron of the nearest-neighbor atoms is the smallest part of the unit cell that can be used to obtain the relaxed atomic positions in the lattice. Without lattice relaxation effects its size is independent of its composition, i.e., of the number of atoms of different types it contains, and thus all interatomic distances are the same. If we now allow the atoms to relax to their equilibrium positions, they will move in such a way, that the distances between the atoms in the three different configurations, A-A, A-B and B-B, will be different from each other and from that of the unrelaxed case. To find these distances we then apply the simple spring model described in Ref. 23 that predicts nearest neighbor distances in a reasonably good agreement with experimental data.[46]

In our model the relaxation energy associated with such changes of the interatomic distances is just the difference between the total energy of the tetrahedron at the unrelaxed average alloy volume Ω_0 and at the volume given by the relaxed interatomic distances Ω_{rel}:

$$E_{rel} = E_{tot}(\Omega_0) - E_{tot}(\Omega_{rel}), \qquad (7)$$

where all the energies are determined per atom.

The actual total energy calculations are based on five possible arrangements of atoms in the tetrahedron to which we assign the ordered structures: two pure elements ($4A$ and $4B$), two $L1_2$ structures ($3A1B$ and $3B1A$), and the $L1_0$ structure ($2A2B$). With the relaxation energy assigned to each tetrahedron during the Monte Carlo simulation one can obtain the relaxation energy for each particular atomic distribution in the sample. In order to derive the relaxation en-

ergy of a random alloy one can carry out Monte Carlo simulations at a very high temperature where the SRO effects become negligible.

G. Monte Carlo simulations for the bulk

A 32 768-atom box ($32 \times 32 \times 32$) with periodic boundary conditions has been used in the bulk Monte Carlo simulations. Test simulations performed for a larger 64 000-atom cell indicates good convergence with the size of the simulation cell. During the simulations the energy ΔE of the exchange of two randomly chosen atoms of different sorts was calculated and the asymmetric Metropolis algorithm[47] was used to decide whether one should exchange the atoms or not.

The simulation process was started at a temperature sufficiently well above the ordering transition temperature T_c and the cell was initially filled with randomly distributed Ni and Pt atoms. The temperature was subsequently lowered by 50 K after 5000 attempts of exchange trials per atom. The total energy, pair-correlation functions, and structure factors were collected and averaged over the last 1000 steps. A jump in the temperature dependence of the total energy indicates a phase transition, and the stored correlation functions, structure factors, and positions of the atoms in real space allow one to determine the nature of the ordered structure obtained.

H. DEMC method for surfaces

The simplest way to calculate a surface-concentration profile is to use the Monte Carlo method in the canonical ensemble approach with a fixed number of atoms of different types.[48,49] In this case two boundaries with vacuum are considered as independent surfaces and the middle of the slab represents bulk. However, this scheme is computationally costly since the thickness of the slab should be large, in practice approximately 100 layers, in order to avoid possible mutual influence of the surfaces and to keep an approximately constant concentration in the middle layers.

The problem with the size of the simulation box can be solved if one uses the grand canonical ensemble in the Monte Carlo simulations. In this case, however, one needs in general to know the chemical potential $\mu(T) = dF(T)/dc|_{c=c_b}$ of the bulk at a given temperature. Two different ways to deal with this problem have been proposed in the literature. In a number of papers[50–53] the surface has been supplied with bulk atoms via several layers near the bulk-surface boundary, at which a random alloy with the

TABLE I. The enthalpies of formation (in mRy) of random and ordered $L1_0$ NiPt alloys obtained by different methods.

Method	ΔH_{rand}^0	ΔH_{rand}^{rel}	$\Delta H_{L1_0}^0$	$\Delta H_{L1_0}^{rel}$
KKR-(CPA)-ASA+M (LSGF)	1.57	-1.03	-6.06	
CWM-FP-LAPW (Ref. 44)	1.72	-2.23	-5.71	-7.03
CWM-FP-LMTO (Ref. 23)	~ 1.0		-8.7	
Exp. (Ref. 59)				-7.06

TABLE II. The effective pair interactions (in K) and ordering energy (in mRy) for NiPt at a fixed lattice constant.

Method	$V^{(2,1)}$	$V^{(2,2)}$	$V^{(2,3)}$	$V^{(2,4)}$	$E_{ord}^{L1_0}$
CWM-ASA+M	3087	161	119	-175	-7.58
SGPM	3337	38	-521	-418	-8.34

bulk concentration was fixed during the simulation process. In fact, a mean-field chemical potential has been used, and, therefore, this technique could work well only at temperatures well above T_c. Another technique[54–56] uses the chemical potential determined from bulk MC simulations. By performing MC simulations for different values of μ one may obtain the dependence of the concentration c upon $\mu(T)$. Thus, one may calculate the value of μ for a given value of c and T. However, this technique requires several bulk simulations for each temperature.

In the present work we have developed the DEMC method which is a grand canonical ensemble technique that requires no knowledge of the chemical potential in the bulk. The idea of the method is to use the simulation box, initially calculated by the usual Monte Carlo method, as a reservoir for supplying atoms to the surface. In this case the trial energy in the DEMC simulations is

$$\Delta E = \Delta E_s(A \rightarrow B) + \Delta E_b(B \rightarrow A), \qquad (8)$$

where $\Delta E_s(A \rightarrow B)$ is the change in the total energy of the surface sample due to the change of a randomly chosen atom from A to B and $\Delta E_b(B \rightarrow A)$ is the change in the total energy of the previously equilibrated bulk sample due to the change of a randomly chosen atom from B to A. The usual Metropolis algorithm is applied, and, if the decision to change has been made, the type of atom is changed at the *surface* only. This is justified by the general rule that no change at a surface can affect the thermodynamical state of the bulk, since the bulk is considered as infinitely large compared to the surface.

Our computational procedure was as follows. First bulk MC simulations are performed for several temperatures and the final distributions of atoms are stored. Then surface DEMC simulations start at the same temperature. The periodic conditions are applied at the surface sample only on boundaries that are perpendicular to the surface. At the bulk-surface interface we use a cut of the bulk MC sample by planes parallel to the surface with the thickness of several layers as the boundary. Bulk periodic boundary conditions are applied, if necessary, to make this cut cover the whole bulk-surface boundary. We have used the 28×28 and 32×32 samples with the thickness of 40 and 28 layers for the (110) and (111) surfaces, respectively, with 31 360 atoms for the (110) surface and 28 672 atoms for the (111) surface. We use 5000 exchange trials per atom at each temperature, and the concentration profiles are averaged over the last 1000 steps.

III. CONFIGURATIONAL THERMODYNAMICS OF BULK NIPT

A. Ground-state properties and effective interactions

The KKR-(CPA)-ASAM method with screened Madelung potential and energy deduced from the locally self-consistent Green's-function technique,[57] as described in Ref. 22, has been used to calculate the equilibrium lattice spacing and the total energy of a Ni$_{50}$Pt$_{50}$ random alloy and of the $L1_0$ ordered phase. The calculated values of the equilibrium lattice spacing of 3.733 Å for the random alloy and 3.719 Å for the ordered alloy [the tetragonal distortion of $c/a \sim 0.94$ (Ref. 58) have not been considered] are in a very good agreement with the room-temperature experimental data of 3.749 Å and 3.73 Å (on average), respectively.[58]

In Table I we present the enthalpies of formation of the random and $L1_0$ ordered equiatomic NiPt alloys calculated by different techniques together with experimental data. The values of the enthalpies for a relaxed random alloy ΔH_{rand}^{rel} in this work have been obtained by adding the relaxation energy (-2.6 mRy, calculated in the effective tetrahedron volume approach) to the enthalpy of formation of the unrelaxed random alloy presented in the first column of the Table. It is in reasonable agreement with the value -3.96 mRy found by Lu *et al.*[44] in the full-potential calculations by the Connolly-Williams method. It is clear that the overall agreement of the KKR-(CPA)-ASA+M results with the results obtained by more sophisticated techniques is very good.
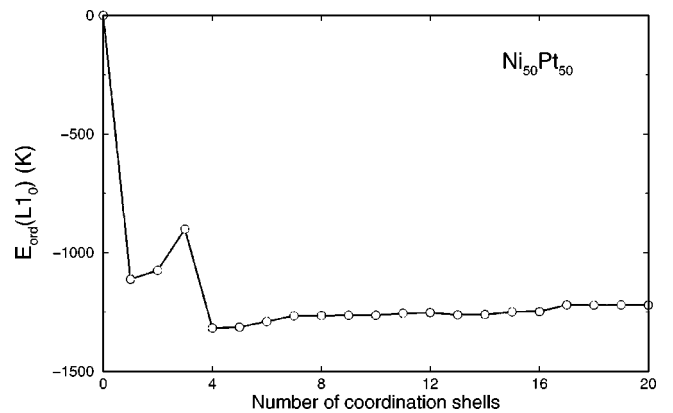
FIG. 1. The ordering energy E_{ord} (in K) of the $L1_0$ structure as a function of the number of coordination shells included in the calculation.
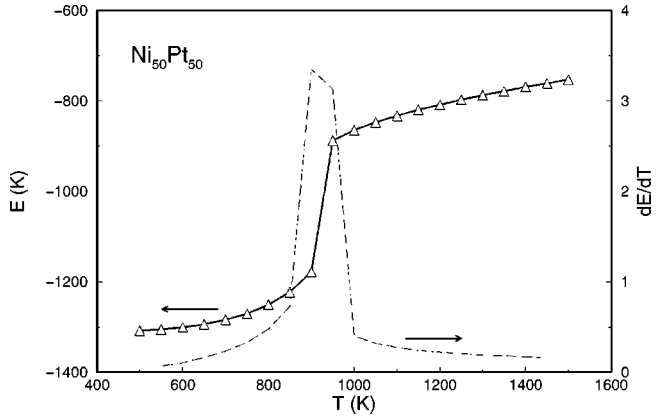
FIG. 2. The configurational energy per atom $E(K)$ of the $Ni_{50}Pt_{50}$ alloy (solid line) and its first temperature derivative dE_{conf}/dT (dashed line) as a function of temperature in the Monte Carlo simulations. Triangles represent points at which the Monte Carlo simulations have been performed. The energy scale is shown on the left-hand side of the picture, and the scale of the first energy derivative on the right-hand side.

FIG. 3. The calculated Warren-Cawley SRO parameters a_{lmn} at the first seven coordination spheres (open diamonds). The experimental SRO (open circles) data are from Ref. 61.

The calculations of the effective interactions have been carried out for a lattice parameter of 3.79 Å, which corresponds to that of a random alloy at temperatures above 1000 K estimated in the Debye-Grüeisen model.[60,40] In Table II we present the first four effective pair interactions, calculated by means of CWM-ASA+M and SGPM, as well as the ordering energy of the $L1_0$ structure calculated from these interactions. All methods give very similar values for the largest pair interaction $V^{(2,1)}$ at the first coordination shell. Although the CWM-ASA+M interactions for more distant coordination shells fall off quite rapidly in contrast to the SGPM potentials, it is very likely that this is due to a renormalization of the CWM interactions because of the neglect of the more distant interactions, as demonstrated below.

In Fig. 1 we show the $L1_0$ ordering energy as a function of the number of SGPM interactions included in the calculations. One finds that the first four interactions presented in Table I give the value of -8.35 mRy (-1319 K), which is about 1 mRy lower than the values of the ordering energy obtained in the Connolly-Williams calculations. However, if we continue the summation of the SGPM interactions further the ordering energy goes up: It is equal to -8.01 mRy (-1265 K) when the first seven interactions are included and -7.73 mRy (-1221 K) with the 17 interactions, which is very close to the CWM results. Thus, the lower values of the CWM interactions could be a renormalization effect.

We have also calculated the three- and four-site interactions and found them to be quite small. For instance, the effective cluster interaction that corresponds to the triangle of the nearest neighbors is about 150 K, and the effective interaction for the tetrahedron of the nearest neighbors is less than 10 K. Therefore multisite interactions have been excluded from further consideration.

B. Transition temperature and the short-range order parameters

As has been shown in the preceding section, the SGPM interactions reproduce quite well the ordering energy of the $L1_0$ structure. These interactions have been used in the Monte Carlo simulations together with the effective tetrahedron volume approach for treating lattice relaxation effects. In Fig. 2 we show the total energy per atom and its temperature derivative in the Monte Carlo simulations with effective pair interactions included up to the seventh coordination shell as a function of temperature. The phase transition to the ordered $L1_0$ structure occurs between 900 K and 950 K, in excellent agreement with the experimental data, 918 K. The calculated values of the Warren-Cowley SRO[37] parameters at 1200 K are quite close to those measured at the same temperature.[61] The first seven calculated and measured Warren-Cowley SRO parameters versus distance $r_{lmn} = a/2(l^2+m^2+n^2)^{1/2}$ (where a is the lattice parameter) are plotted in Fig. 3. If we now include the SGPM interactions only for the first four coordination shells in the Monte

TABLE III. The surface energies of pure Ni and Pt in J/m^2 (eV/atom) calculated at their equilibrium lattice parameters and at the equilibrium lattice parameter of $Ni_{50}Pt_{50}$ random alloy. Experimental data for pure Ni and Pt are taken from (Ref. 62).

	Components lattice parameters			Alloy lattice parameter	
	(110)	(111)	Exp.	(110)	(111)
Ni	3.12 (1.64)	2.82 (0.91)	2.45	2.55 (1.62)	2.17 (0.84)
Pt	2.95 (2.01)	2.60 (1.08)	2.48	2.71 (1.72)	2.44 (0.95)

TABLE IV. The effective interactions for Ni$_{50}$Pt$_{50}$ (111) (in K).

	λ			
	1	2	3	4(bulk)
$V_\lambda^{(1)} - V_{bulk}^{(1)}$	-705	231	-219	0
$V_{\lambda\lambda+n}^{(2,s)}$				
			$s=1$	
$n=0$	1373	1852	1979	1668
1	1927	1857	1668	1668
			$s=2$	
1	82	-33	38	38
			$s=3$	
0	-143	-167	-181	-130
1	-233	-339	-260	-260
2	-151	-130	-130	-130
			$s=4$	
0	-138	-207	-177	-209
2	-222	-209	-209	-209

Carlo simulations, the transition temperature increases to 1050 K, which is still in a very good agreement with experiment. This means that we can actually restrict ourselves to the first four pair interactions to reproduce correctly the configurational state of the alloys near the surface.

IV. SURFACE SEGREGATION ENERGIES

The difference in the surface energies of the pure alloy components may sometimes be a good estimate for the corresponding surface segregation energies. In Table III we show the calculated values of the surface energies of pure Ni and Pt for the (111) and (110) surfaces and compare them with experimental data.[62] It is obvious that the surface energies of Ni and Pt for these surface orientations are too close to each other to draw any conclusions concerning segregation.

It has been argued in Ref. 63 that in order to estimate the contribution from an impurity to the surface energy one needs to compare the surface energies of an impurity com-

TABLE V. The effective interactions for Ni$_{50}$Pt$_{50}$ (110) (in K).

	λ				
	1	2	3	4	5(bulk)
$V_\lambda^{(1)} - V_{bulk}^{(1)}$	168	-883	-265	163	0
$V_{\lambda\lambda+n}^{(2,s)}$					
			$s=1$		
$n=0$	483	555	571	586	556
1	2433	2286	2379	2224	2224
2	781	686	556	556	556
			$s=2$		
0	-3	38	13	18	13
2	57	33	25	25	25
			$s=3$		
0	-116	-96	-116	-117	-87
1	-163	-215	-184	-173	-173
2	-77	-109	-106	-87	-87
3	-161	-174	-174	-174	-174
			$s=4$		
0	-41	-476	-68	-71	-70
2	301	-283	-278	-278	-278
4	-70	-70	-70	-70	-70

ponent and a host component calculated at the lattice parameter of the host. If one considers Ni and Pt atoms as ''impurities'' in the $Ni_{50}Pt_{50}$ host, the alloy component with the lower surface energy at the lattice constant of the $Ni_{50}Pt_{50}$ alloy is expected to segregate. In Table III we also include the surface energies of the (110) and (111) facets of pure Ni and Pt calculated at the lattice spacing of the random $Ni_{50}Pt_{50}$ alloy. However, again the differences between the Ni and Pt surface energies are too small, especially for the (110) surface, to predict the surface segregation in NiPt.

The direct calculations of the surface segregation energies, or the on-site effective interactions $V_\lambda^{(1)} - V_{bulk}^{(1)}$, give the results that are presented in Tables IV and V in the basis of spin variables with the convention that $\sigma_i = 1$ if site i is occupied by a Pt atom. Therefore, the negative sign of $V_\lambda^{(1)} - V_{bulk}^{(1)}$ favors a Pt segregation towards the layer λ, and vice versa. Thus, in the case of the (111) surface one should expect a pronounced Pt segregation towards the surface, and vice versa a weak Ni segregation toward the (110) surface. It is quite interesting that the surface segregation energy for the second layer of the (110) surface is almost one order of magnitude larger than that for the first layer and has the opposite sign, corresponding to Pt segregation.

Although the present result differs somewhat from the one presented in the first LMTO-CPA calculations by Abrikosov *et al.*,[16] where the segregation energy was found to be negative for both the first two layers of the (110) surface, it does not change the overall qualitative picture: The dominating segregation in both cases is the Pt segregation into the second layer. Besides, although the segregation energy into the first layer is positive in the present study, favoring Ni segregation, the value of 167 K is too small to induce a segregation at 1300 K. Indeed the surface segregation calculations with only on-site interactions included in the Hamiltonian, which are presented in Fig. 4, show that the segregation energy $V_1^{(1)} - V_{bulk}^{(1)}$ for the (110) surface practically does not lead to surface segregation of Ni.

V. EFFECTIVE PAIR INTERACTIONS FOR SURFACES

We have calculated the surface effective pair interactions, Eq. (2), using the supercell geometry and the SGPM technique as described in Ref. 22. Since the number of interactions increases dramatically in the case of surfaces, we have taken into consideration only pair interactions at the first four coordination shells that, as has been shown in Sec. III B, reproduce quite well the ordering transition in NiPt. The interactions for layers deeper than the fourth in the case of the
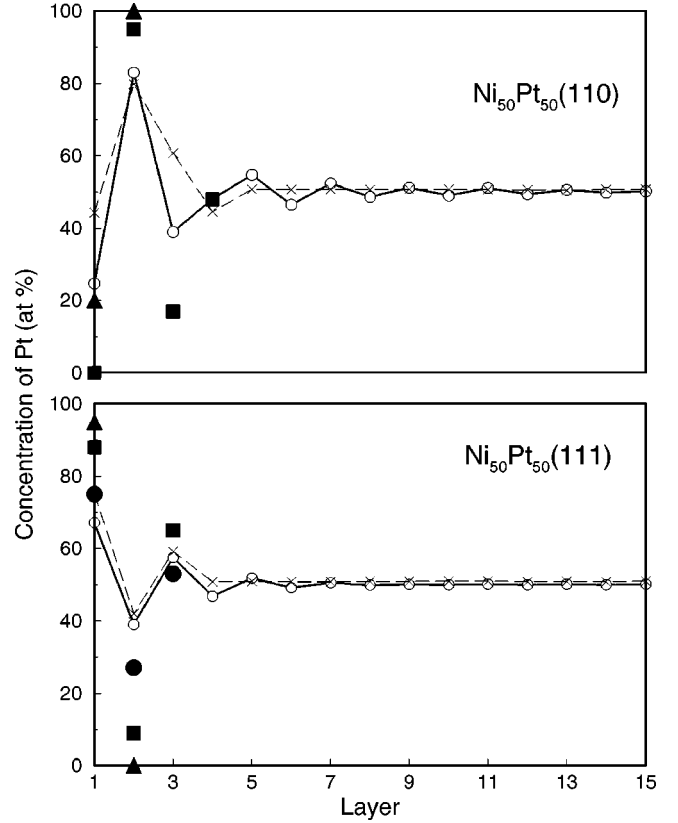
FIG. 4. The surface segregation profiles of the $Ni_{50}Pt_{50}$ alloy at the (110) (upper panel) and (111) (lower panel) surfaces. The calculated profiles are shown by a solid line. The dashed line shows the profile calculated from only on-site interactions. The filled triangles, squares, and circles represent the results of the IDEAS,[5] LEED,[1,2] and MEIS[7] measurements, respectively.

(110) surface and the third in the case of the (111) surface have been set equal to the corresponding bulk counterparts.

It is interesting to notice that the pair interactions at the surface, presented in Tables IV and V, only slightly deviate from the corresponding bulk interactions (given for the last layer). One may also notice that, in fact, the effective interactions for the (110) surface differ substantially from those for the (111) surface. For instance, the *intralayer* effective interactions at the first coordination shell for the (111) surface $V_{\lambda\lambda}^{(2,1)}$ are three times as large as those for the (110) surface. On the other hand the nearest-neighbor *interlayer* interactions, $V_{\lambda\lambda+1}^{(2,1)}$ are much larger at the (110) surface.

Such a difference has a geometrical nature: The effective interactions presented are those that are used in the total

TABLE VI. The layer-resolved coordination numbers $Z_{\lambda\lambda+n}^{(s)}$ for the fcc(110) and (111) surfaces.

s	bulk	fcc(110)					fcc(111)		
		$n=0$	1	2	3	4	0	1	2
1	12	2	8	2			6	6	
2	6	2		4				6	
3	24	4	8	4	8		6	12	6
4	12	2		8		2	6		6

energy expansion (2) where the summation over coordination shells has already been carried out, and thus they are proportional to the layer resolved coordination numbers $Z_{\lambda\lambda+n}^{(s)}$, which are the numbers of the atoms in the sth coordination shell in the $\lambda+n$ layer for the atoms in the λ layer. They are given in Table VI. This means that the strong interlayer ordering in the case of (110) surface, as compared to the (111) surface, has a geometrical origin. In fact, in the case of the completely ordered $L1_0$ structure, all (the 111) layers have the same equiatomic composition, while all (110) layers form a sequence of pure Pt and Ni layers.

VI. SURFACE-CONCENTRATION PROFILES

The effective interactions described above have been used in DEMC simulations in the temperature range between 500 and 1500 K. Lattice relaxation effects have been taken into account by the effective tetrahedron method as in the bulk MC simulations, while the effect of surface relaxation was neglected. Although it is probably still a reasonably good approach in the case of the closed-packed (111) surface, it might be insufficient for the much more open (110) surface, especially in the case of an oscillatory concentration profile. However, we believe that the chemical interactions play a major role in the case of (110) surface and we will comment on this below.

In Fig. 4 we present the calculated segregation profiles at 1300 K together with experimental data[1,2,5] obtained in the temperature interval 1120–1170 K. We have increased the temperature in the theoretical simulations by 150 K because our ordering temperature T_c obtained with the first four pair interactions is 150 K higher than the experimental one. It is clear that the theoretical results are in good agreement with the experiment. The somewhat underestimated oscillatory behavior of the surface concentration profile for the (110) surface is most probably due to the neglected interlayer relaxations [a large contraction of the interlayer distance of about 19% at the (110) surface is found by Lundberg[64]] specific for this surface. Additional interlayer relaxations should lower the total energy of the system with alternating Ni-Pt-Ni- layers and thus in effect increase the interlayer interactions. This should lead to a more pronounced oscillatory behavior of the surface concentration profile.

It is important to note that in agreement with the findings in Ref. 16, the so-called segregation reversal at the (110) surface, i.e., the Ni segregation toward this surface, is basically caused by the strong Pt segregation into the second layer of this surface together with a pronounced interlayer ordering. This can clearly be seen in Fig. 4 if one compares the surface-concentration profiles for this surface calculated with and without effective pair interactions. As has been

mentioned above, on the one hand the surface segregation energies alone do not lead to this effect, and on the other hand, the strong interlayer ordering cannot lead to the oscillatory behavior of the surface-concentration profiles above the order-disorder transition without preferential segregation of an alloy component at least into one layer within the surface region.

VII. SUMMARY

A combination of different *ab initio* and statistical mechanics techniques have been used to calculate the configurational thermodynamics of bulk and surface Ni$_{50}$Pt$_{50}$ alloys. The effective cluster interactions have been obtained by the screened generalized-perturbation method, and verified by the Connolly-Williams method for bulk alloys. The Monte Carlo method has been applied in the statistical thermodynamic simulations, which in the case of surfaces have been generalized to the direct-exchange Monte Carlo method in the grand canonical ensemble. Lattice relaxation effects have been taken into account by the effective volume tetrahedron approach.

The results obtained may be summarized as follows

(1) The enthalpies of formation of random and ordered NiPt alloys calculated by means of the KKR-(CPA)-ASA+M method agree reasonably well with the results of the full potential calculations.

(2) The SGPM interactions combined with the effective volume approach in the Monte Carlo simulations provide a quite accurate description of the configurational thermodynamics in the bulk: the SRO parameters and the order-disorder transition temperature agree well with experiment.

(3) The calculated surface-concentration profiles are in satisfactory agreement with the experimental data indicating Pt enrichment at the (111) surface and Ni enrichment at the (110) surface. The analysis of the effective interactions leads to the conclusion that the segregation reversal at the (110) surface is due to a combination of the strong Pt segregation into the subsurface layer and interlayer ordering, which is a consequence of the geometrically amplified ordering tendency in NiPt.

[1] Y. Gauthier, Y. Joly, R. Baudoing, and J. Rundgren, Phys. Rev. B **31**, 6216 (1985).

[2] Y. Gauthier, R. Baudoing, M. Laundgren, and J. Rundgren, Phys. Rev. B **35**, 7867 (1987).

[3] Y. Gauthier, R. Baudoing, and J. Jupille, Phys. Rev. B **40**, 1500 (1989).

[4] Y. Gauthier and R. Baudoing, in *Surface Segregation Phenomena*, edited by P. A. Dowben and A. Miller (CRC, Boca Raton,

FL, 1990).

[5] D. Dufayard, R. Baudoing, and Y. Gauthier, Surf. Sci. **233**, 223 (1990).

[6] Y. Gauthier, W. Hoffmann, and M. Wuttig, Surf. Sci. **233**, 239 (1990).

[7] S. Deckers, F.H.P.M. Habraken, W.F. van der Weg, A.W. Denier van der Gonm, B. Pluid, J.F. van der Veen, and R. Baudoing, Phys. Rev. B **42**, 3253 (1990).

[8] P. Weigand, P. Novacek, G. VanHusen, T. Neidhart, and P. Varga, Surf. Sci. **269/270**, 1129 (1992).

[9] P. Weigand, W. Hofer, and P. Varga, Surf. Sci. **287/288**, 350 (1993).

[10] P. Weigand, B. Jelinek, W. Hofer, and P. Varga, Surf. Sci. **301**, 306 (1994).

[11] H. Stadler, W. Hofer, M. Schmid, and P. Vagra, Surf. Sci. **287/288**, 366 (1993).

[12] G. Tréglia and B. Legrand, Phys. Rev. B **35**, 4338 (1987).

[13] B. Legrand, G. Tréliga, and D. Ducastelle, Phys. Rev. B **41**, 4422 (1990).

[14] P. Deurinck and C. Creemers, Surf. Sci. **441**, 493 (1999).

[15] W. Hofer and L.Z. Mezey, Mikrochim. Acta **125**, 93 (1997).

[16] I.A. Abrikosov, A.V. Ruban, H.L. Skriver, and B. Johansson, Phys. Rev. B **50**, 2039 (1994).

[17] J.W.D. Connolly and A.R. Williams, Phys. Rev. B **27**, 5169 (1983).

[18] A.V. Ruban, I.A. Abrikosov, D. Ya. Kats, D. Gorelikov, K.W. Jacobsen, and H.L. Skriver, Phys. Rev. B **49**, 11 383 (1994).

[19] H.L. Skriver and N.M. Rosengaard, Phys. Rev. B **43**, 9538 (1991).

[20] I.A. Abrikosov and H.L. Skriver, Phys. Rev. B **47**, 16 532 (1993).

[21] A.V. Ruban, I.A. Abrikosov, and H.L. Skriver, Phys. Rev. B **51**, 12 958 (1995).

[22] A.V. Ruban and H.L. Skriver (unpublished).

[23] C. Amador, W.R.L. Lambrecht, M. van Schilfgaarde, and B. Segal, Phys. Rev. B **47**, 15 276 (1993); C. Amador and G. Bozzolo, *ibid.* **49**, 956 (1994).

[24] P. Hohenberg and W. Kohn, Phys. Rev. B **136**, 864 (1964); W. Kohn and L.J. Sham, Phys. Rev. A **140**, 1133 (1965).

[25] O.K. Andersen, Phys. Rev. B **12**, 3060 (1975); O. Gunnarsson, O. Jepsen, and O.K. Andersen, *ibid.* **27**, 7144 (1983).

[26] P. Soven, Phys. Rev. **156**, 809 (1967).

[27] B.L. Gyiörffy, Phys. Rev. B **5**, 2382 (1972).

[28] J.S. Faulkner, Prog. Mater. Sci. **27**, 1 (1982).

[29] P.A. Korzhavyi, I.A. Abrikosov, B. Johansson, A.V. Ruban, and H.L. Skriver, Phys. Rev. B **59**, 11 693 (1999).

[30] A.V. Ruban and H.L. Skriver, Comput. Mater. Sci. **15**, 119 (1999).

[31] H.L. Skriver and N.M. Rosengaard, Phys. Rev. B **46**, 7157 (1992).

[32] L. Vitos, B. Johansson, J. Kollar, and H.L. Skriver, Phys. Rev. A **61**, 052511 (2000); Phys. Rev. B **62**, 10 046 (2000).

[33] N. Kawamiya and K. Adachi, Trans. Jpn. Inst. Met. **16**, 327 (1975).

[34] D.D. Koelling and B.N. Harmon, J. Phys. C **10**, 3107 (1977).

[35] N.E. Christensen and S. Satpathy, Phys. Rev. Lett. **55**, 600 (1985).

[36] J.M. Sanchez, F. Ducastelle, and D. Gratias, Physica A **128**, 334 (1984); J. M. Sanchez and D. de Fontane, *Structure and Bonding in Crystals* (Academic, New York, 1981), p. 117.

[37] F. Ducastelle, *Order and Phase Stability in Alloys* (North-Holland, Amsterdam, 1991).

[38] P.E.A. Turchi, G.M. Stocks, W.H. Butler, D.M. Nicholson, and A. Gonis, Phys. Rev. B **37**, 5982 (1988); P.P. Singh and A. Gonis, *ibid.* **47**, 6744 (1993); P.P. Singh, A. Gonis, and P.E.A. Turchi, Phys. Rev. Lett. **71**, 1605 (1993).

[39] V. Drchal, J. Kudrnovský, L. Udvardi, P. Weinberger, and A. Pasturel, Phys. Rev. B **45**, 14 328 (1992); A. Pasturel, V. Drchal, J. Kudrnovský, and P. Weinberger, *ibid.* **48**, 2704 (1993); V. Drchal, J. Kudrnovsky, A. Pasturel, I. Turek, and P. Weinberger, *ibid.* **54**, 8202 (1996).

[40] P.A. Korzhavyi, A.V. Ruban, S.I. Simak, and Yu.Kh. Vekilov, Phys. Rev. B **49**, 14 229 (1994).

[41] W. Schweika and A.E. Carlson, Phys. Rev. B **40**, 4990 (1989).

[42] Z.W. Lu, S.-H. Wey, A. Zunger, S. Frota-Pessoa, and L.G. Ferreira, Phys. Rev. B **44**, 512 (1991).

[43] A.V. Ruban and H.L. Skriver, Phys. Rev. B **55**, 8801 (1997).

[44] Z.W. Lu, S.-H. Wei, and A. Zunger, Europhys. Lett. **21**, 221 (1993).

[45] V. Ozolins, C. Wolverton, and A. Zunger, Phys. Rev. B **57**, 6427 (1998).

[46] G. Renaud, N. Motta, F. Lancon, and M. Belakhovsy, Phys. Rev. B **38**, 5944 (1988).

[47] K. Binder, *Applications of the Monte Carlo Method in Statistical Physics* (Springer, Berlin, 1984)

[48] K.S. Lee, S.H. Kim, H.G. Min, J. Seo, and J.S. Kim, Surf. Sci. **377-379**, 918 (1997).

[49] W. Schweika, P.D. Landau, and K. Binder, Phys. Rev. B **53**, 8937 (1996).

[50] V.S. Sundaram and P. Wynblatt, Surf. Sci. **52**, 569 (1975).

[51] R.G. Donnely and T.S. King, Surf. Sci. **74**, 89 (1978).

[52] J. Eymery and J.C. Joud, Surf. Sci. **231**, 419 (1990).

[53] A. Pasturel, V. Drchal, J. Kudrnovský, and P. Weinberger, Phys. Rev. B **48**, 2704 (1993).

[54] S.M. Foiles, Phys. Rev. B **32**, 7685 (1985).

[55] A. Seki, D.N. Seidman, Y. Oh, and S.M. Foiles, Acta Metall. Mater. **39**, 3167 (1991).

[56] D. Udler and D.N. Seidman, Acta Metall. Mater. **42**, 1959 (1994).

[57] I.A. Abrikosov, A.M.N. Niklasson, S.I. Simak, B. Johansson, A.V. Ruban, and H.L. Skriver, Phys. Rev. Lett. **76**, 4203 (1996); I.A. Abrikosov, S.I. Simak, B. Johansson, A.V. Ruban, and H.L. Skriver, Phys. Rev. B **56**, 9319 (1997).

[58] W. B. Pearson, *A Handbook of Lattice Spacing and Structure of Metals and Alloys* (Pergamon Press, London, 1967).

[59] R. Hultgren, P. D. Desal, D. T. Hawkins, M. Gleiser, and K. K. Kelley, *Selected Values of the Thermodynamic Properties of Binary Alloys* (ASM, Metals Park, OH, 1973).

[60] V.L. Moruzzi, J.F. Janak, and K. Schwarz, Phys. Rev. B **37**, 790 (1988).

[61] D.K. Saha and K. Ohshima, J. Phys.: Condens. Matter **7**, 3203 (1995).

[62] F. R. de Boer, R. Boom, W. C. M. Mattens, A. R. Miedema, A. K. Niessen, *Cohesion in Metals* (North-Holland, Amsterdam, 1988).

[63] M. Alden, I. A. Abrikosov, B. Johansson, N. M. Rosengaard, and H. L. Skriver, Phys. Rev. B **50**, 5131 (1994).

[64] M. Lundberg, Phys. Rev. B **36**, 4692 (1987).